Radon and Mojette Projections' Equivalence
for Tomographic Reconstruction using Linear Systems

Benoît RECUR

LaBRI, University of Bordeaux 1

351 cours de la Libération

33405 Talence Cedex, France

benoit.recur@labri.fr

Pascal DESBARATS

LaBRI, University of Bordeaux 1

351 cours de la Libération

33405 Talence Cedex, France

pascal.desbarats@labri.fr

Jean-Philippe DOMENGER

LaBRI, University of Bordeaux 1

351 cours de la Libération

33405 Talence Cedex, France

jean-philippe.domenger@labri.fr

ABSTRACT

In medical imaging, the Radon transform, used for tomographic reconstruction, recovers a N-Dimensional image from a set of acquired (N-1)D projections. However, it implies approximations in discrete domain. Beside this transform, Mojette transform has been developped as a discrete and exact transform. However, its construction is incompatible with physical X-Rays properties. In this paper, after having recalled generalities about both transforms, we introduce the conditions under which their projections are equivalent and how to reconstruct an image with the Mojette backprojection from a Radon acquisition using linear systems. This method will be applied on some examples and results will be compared with usual Radon transform.

Keywords: Radon Transform, Mojette Transform, Tomography, Reconstruction, Linear Systems

1 INTRODUCTION

X-Rays form an electromagnetic wave which has a wavelength much higher than visible light. This property allows it to go through matter. In this process, the X-Ray beam undergoes an attenuation proportional to the density of the traversed matter. It is the basic principle for X-Ray radiography.

In medical or industrial CT scanner, a 2D slice of the imaged object is acquired by casting X-Rays following several angles around the object. For each angle, the attenuation of the X-Rays beam is measured leading to a 1D projection of the object. The 2D slice is then reconstructed from a set of projections [7] using the Radon theorem [11]. The main drawback of this method is that the Radon theorem is defined in the continuous domain whereas images are in the discrete domain [5].

Two different approaches can be followed to overcome this problem. The first one is to try to improve reconstructed image quality by signal filters and the second one is to directly implement discrete reconstructions. In this article, we firstly introduce the Radon theorem, its discrete implementation and its limitations. Secondly, we present a direct discrete transform called the Mojette Transform [4]. This transform is exact which means that there is no difference between origi-

nal and reconstructed images but its acquisition method is slightly different from a classical CT scan acquisition. Then, we expose the modelisation of the physical acquisition in order to extract acquisition parameters to make it compatible with an exact reconstruction transform. Finally, we present results and comparisons between this method and different classical reconstruction transforms.

2 RECONSTRUCTION METHODS

2.1 Radon Transform

The direct Radon Transform (RT) maps a discrete image data $I(k,l)$ into a set of discrete projections RT_θ. This set of projections is called a sinogram. It allows to recover the two dimensional domain by applying the inverse Radon Transform (RT^{-1}) [15]. The RT of a two dimensional discrete function $I(k,l)$ is defined by :

$$RT_\theta(\rho) = \sum_{-\infty}^{+\infty}\sum_{-\infty}^{+\infty} I(k,l) kernel(\rho - kcos\theta + lsin\theta) \quad (1)$$

where :

- θ and ρ are respectively the angular and radial coordinates of the projection line,

- $I(k,l)$ is the value of pixel of coordinates (k,l).

The kernel of this discrete transform is determined by the pixel model used. Typically, this *kernel* is the discrete Dirac impulse which considers with the same importance each pixel traversed by the projection line :

$$\Delta(x) = \begin{cases} 1 & \text{if } x = 0 \\ 0 & \text{else} \end{cases}$$

But, an other typical kernel occured from a convolution of two order 0 B-Spline [16, 17] functions (red crenels in figure 1) reflects the manner that each pixel is crossed by a projection line. The projection value depends on the distance travelled in each pixel [6]. This kernel, called $B^0(x)$, is valued as follows :

- 1 if $|x| \leq \frac{\Delta_p(||cos\theta| - |sin\theta||)}{2}$

- $\frac{-2|x| + (|cos\theta| + |sin\theta|)\Delta_p}{2\Delta_p min(|cos\theta|, |sin\theta|)}$
  if $\frac{\Delta_p(||cos\theta| - |sin\theta||)}{2} < |x| \leq \frac{\Delta_p(|cos\theta| + |sin\theta|)}{2}$

- 0 else

where Δ_p is the pixel size.

The trapeze in figure 1 represents the value $B^0(x)$ $(0 \leq B^0(x) \leq 1)$ for a pixel. It is determined according to the distance $x = \rho - kcos\theta + lsin\theta$ between the projection line (θ, ρ) and the parallel which goes through the center of the pixel (k, l). It defines the kernel of the B-Spline Radon transform.
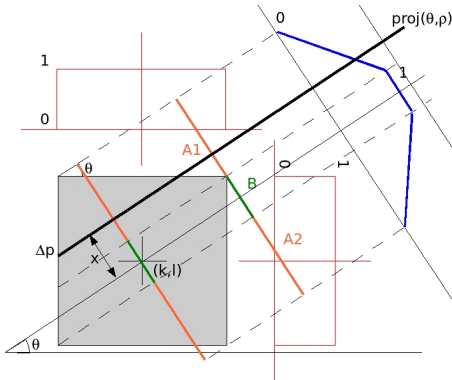

Figure 1: B-Spline 0 kernel

The RT^{-1} function, or commonly named backprojection, recovers $I(k, l)$ domain from projections (Equation 2).

$$I(k, l) = \sum_0^\pi \sum_{-\infty}^\infty RT_\theta(\rho) kernel(\rho - kcos\theta + lsin\theta) \quad (2)$$

2.2 Limits of the Radon Transform

It is obvious that the Dirac impulse leads to approximations, not only in projection computation but also in backprojection, because it considers each pixel with the same maximal coefficient. Figure 2 shows that a projection line travels through a different distance in a pixel, depending on whether this pixel is dark grey or light grey.
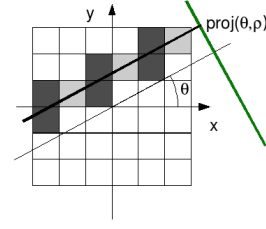

Figure 2: Importance of crossed pixel on a projection line

Furthermore, a sampling on a projection with the two consecutive values shown in figure 3 gives identical results (non unicity of projections).
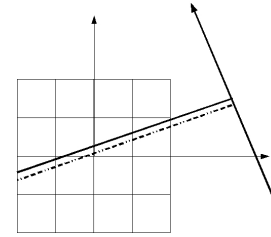

Figure 3: Non unicity of pixel information in a same projection

Using the B-Spline kernel resolves those issues. But other problems remain, due to the sampling (of acquired image or projections) and are independent of the pixel model [1]. A pixel can be considered several times (grey pixel on right scheme on the figure 4) while others only one time (dark grey and light grey pixels) . Another sampling can omit a pixel (grey pixel on the left scheme, figure 4). This problem is well known as irregular sampling.
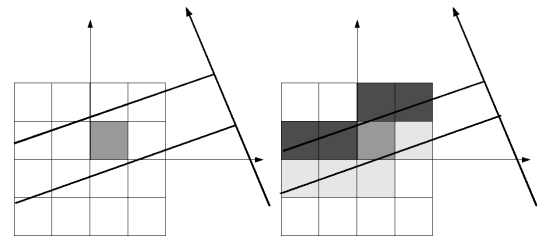

Figure 4: Irregular sampling on the projections

2.3 Radon Results and Existing Optimisations

We consider the following image (Figure 5) which represents the Shepp-Logan phantom [14]. We perform the RT acquisition with B-Spline kernel of this image for sampling step between two projection lines of $d_\rho = 0.5$ (i.e. the distance between each line is twice smaller then a pixel size) and for $N_\theta = 180$ projections. So, the step between each angle is $d_\theta = 1$. The obtained sinogram

is represented in figure 6. Each line of this sinogram represents the values on a projection. The first line contains values of projection $\theta = 0$, the second line, values of projection $\theta = 1$, and so on.
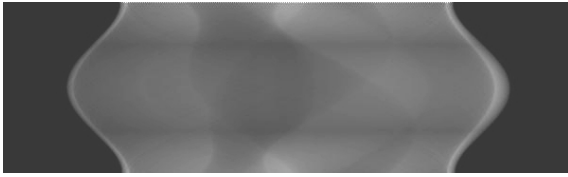

Figure 5: Original image

Figure 6: Sinogram performed with RT and B-Spline kernel for 180 projections and a step of sampling 0.5

This sinogram is used by the RT^{-1} function to reconstruct the image. A consequence of approximations explained above is visible on the result of backprojection : the Radon transform acts as a low-pass filter on the image (left image on the figure 7). Application of a high-pass filter before the backprojection (for example, a ramp filter in 1D Fourier domain of each projection) is often used to reveal details on each projection and to attenuate fuzziness of result image. However, this method well known as "Backprojection of Filtered Projections" (BFP) is not more advised because it increases artefacts (Right image in Figure 7) [15].
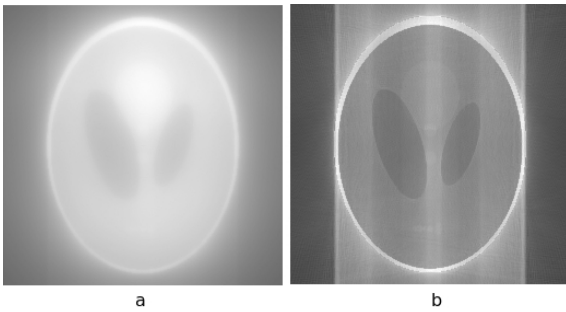

Figure 7: (a) Classic backprojection result, (b) BFP result

2.4 Mojette Transform

The Mojette transform [4, 3] is defined as a discrete version of the Radon transform. It considers only angles $\theta = arctan\frac{q}{p}$ where $p \in Z$ and $q \in Z^+$ are relatively prime ($GCD(p,q) = 1$) and are respectively the number of pixel displacement horizontally and vertically. The Mojette is so given by (Equation 3) :

$$proj_{p,q}(b) = \sum_{-\infty}^{+\infty}\sum_{-\infty}^{+\infty} I(k,l)\Delta(b-kp+lq) \qquad (3)$$

Therefore, the transformed domain consists in projections where each element $proj_{p,q}(b)$, called a bin, is the sum of every pixel intersecting the line $b = kp - lq$. The Mojette transform result is described in figure 8 for a $3*3$ image and for the set of projections $\{(-1,1),(1,1),(1,0)\}$. The number of pixels crossed for each bin is also calculated by applying the Mojette transform to the corresponding unary image. This result will be needed in the inverse Mojette transform algorithm.

The geometry of the Mojette sinogram is defined by p and q. Especially, the number of bins on the projection (p,q) is (for a $w*h$ image) [12] :

$$\#_{bins}(p,q) = (w-1)|p| + (h-1)|q| + 1 \qquad (4)$$

The step between each line of projection is :

$$d_\rho = \frac{1}{\sqrt{p^2+q^2}} \qquad (5)$$

This geometry resolves the Radon sampling problems because sampling properties are defined and adjusted for each projection angles.
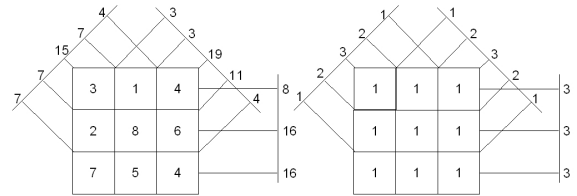

Figure 8: Result of the Mojette transform (on the left) and number of pixels crossed for each bin (on the right)

An image can be recovered if the set of projections follows the Katz criterion. It ensures that the image is reconstructed by the set of projections $P = \{(p_i,q_i), p_i \in Z, q_i \in Z^+, i \in 1...N\}$ if :

$$w \leq \sum_{i=1}^{N}|p_i| \text{ or } h \leq \sum_{i=1}^{N}|q_i| \qquad (6)$$

This set of projections $P = \{(p_i,q_i), p \in Z, q \in Z^+\}$ can be computed automatically with the Farey series [12]. The Farey series of order N, called F_N is the sequence of increasing order of irreducible fractions between 0 and 1 where the denominator is less or equal to N. F_{N+1} is recursively given by F_N including between each successive fractions $\frac{m_i}{n_i}$ and $\frac{m_{i+1}}{n_{i+1}}$ the median fraction $\frac{m_j}{n_j}$ where $m_j = m_i + m_{i+1}$ and $n_j = n_i + n_{i+1}$ if $m_j < N+1$ and $n_j \leq N+1$.

The Farey series gives discrete angles (p,q) by the sequence of fractions $\frac{q}{p}$. Those angles are defined between $[0, \frac{\pi}{4}[$. By symmetries with the first bissecting line and the Y-axis, we obtain the set of projections on $[0, \pi[$.

The inverse Mojette transform back-projects the bins of the different projections onto the reconstructed image. In fact, two Mojette transforms are needed to perform the Mojette backprojection : the Mojette transform of the original image, and the Mojette transform of the unary image in order to know the number of pixels crossed for each bin [4].

This implies that a single pixel bin correspondence must be determined to reconstruct a pixel [4]. Once this has been done, the value of the pixel is subtracted from each projection. The reconstruction of the image is achieved when the total number of pixels has been treated. The first step of this algorithm is shown in the figure 9.
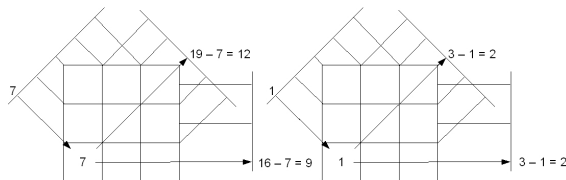

Figure 9: Inverse Mojette transform. On the left : reconstruted image. On the right : correspondence in unary image.

The unary sinogram in the figure 9 shows a pixel correspondence because it contains the value 1. The corresponding bin in the Mojette sinogram contains the value (7) of this pixel. It is reconstructed and its value is subtracted in other bins where it appears. Corresponding bins in unary sinogram are also decreased. Each step of backprojection reconstruct one pixel. So, a $w * h$ image is completely reconstructed in $w * h$ steps.

3 MOJETTE RECONSTRUCTION FROM RADON SINOGRAM

3.1 Differences between Radon and Mojette

The Radon transform uses the same number of samples N_ρ and the same step of sampling d_ρ on each projection. The angle step d_θ between two of them is constant. This method is ideal in medical imaging device. However, we have seen above that its backprojection is approximative and it depends on irregular sampling in discrete domain. The Mojette transform projections are not uniformly projected (d_θ is variable) and the number of bins depends on (p,q). But its backprojection is exact in discret domain.

Consequently, we try to adjust an acquisition with RT according to Mojette properties in order to reconstruct

an image with the Mojette backprojection from a set of projections performed with a Radon acquisition.

3.2 Radon Sinogram Compatible with Mojette Backprojection

The first idea consists to adapt a Radon acquisition to be compatible with Mojette reconstruction. We try in a first place to use the Farey series to define angles and steps of projection lines of the RT acquisition : projection angles are equivalent to Mojette and the number and the step of samples on a projection, too. Call it Radon Farey Transform RFT.

This method gives equivalence between Radon and Mojette projections' geometry. But, the set of pixels crossed by a projection line with Radon defines a discrete line. Only pixels crossed by their center are considered with the Mojette transform (this difference is exposed in Figure 10).
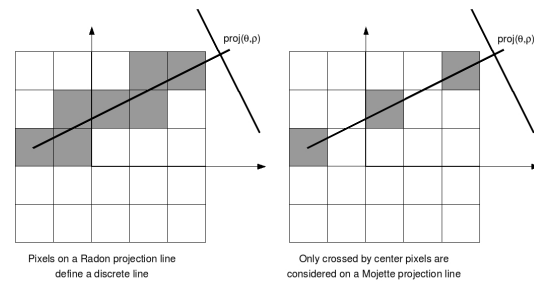

Figure 10: Non equivalence between Radon and Mojette projection line

3.3 Linear System Definition

Consider now the same RFT as above with the B-Spline kernel. We consider firstly a projection value $RFT_\theta(\rho)$ (where $\theta = arctan \frac{q}{p}$) in Radon domain (left scheme on Figure 11) where ρ is equivalent to a bin b in Mojette domain (bin b in the right scheme on Figure 11). This value $RFT_\theta(\rho)$ depends firstly on dark gray pixel values. The sum of these values defines the Mojette value $Moj_{p,q}(b)$ of bin b. But, the value of $RFT_\theta(\rho)$ also depends on gray pixel values. Due to the geometry of acquisition defined by the Farey series and especially the step between two projection lines, the sum of those gray pixel defines the values of neighbouring Mojette bins of b (for example, bins $b-1$ and $b+1$ in the right scheme of Figure 11). Furthermore, the coefficient of these pixels in projections value $RFT_\theta(\rho)$ is defined in the B-Spline kernel according to the distance between their center and the projection line (θ, ρ). But, this coefficient is identical for each pixel in the same neighbouring Mojette bin. Consequently, the consideration of neighbouring Mojette bins in projection $RFT_\theta(\rho)$ is defined according to the distance between projection line (θ, ρ) and neighbouring projection lines (θ, ρ_i).

$RFT_\theta(\rho)$ can be expressed as a linear combination of Mojette bins values.

$$RFT_\theta(\rho) = \alpha_{p,q}(b-i,b) \cdot Moj_{p,q}(b-i) +$$
$$\alpha_{p,q}(b-i+1,b) \cdot Moj_{p,q}(b-i+1) +$$
$$\cdots$$
$$1 \cdot Moj_{p,q}(b) +$$
$$\cdots$$
$$\alpha_{p,q}(b+j,b) \cdot Moj_{p,q}(b+j)$$

where $b \Leftrightarrow \rho$ and $\alpha_{p,q}(b_s,b_t)$ defines B-Spline coefficient between two bins b_s and b_t.

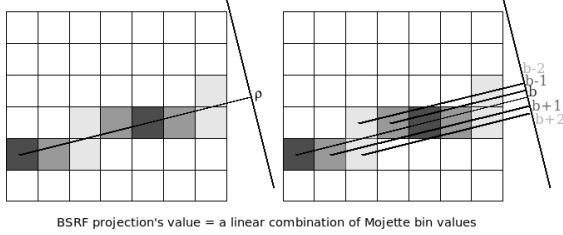BSRF projection's value = a linear combination of Mojette bin values

Figure 11: Linear combination between B-Spline Radon and Mojette projection

The decomposition of a value $RFT_\theta(\rho)$ on a projection is identical for each ρ_i. The N_ρ values measured with the RFT acquisition can be decomposed by a linear combination of bin values in Mojette domain. Consequently, it is possible to set up the following linear system on a projection (p,q) :

$$\begin{cases} RFT_\theta(1) = \alpha_{p,q}(1,1) \cdot Moj_{p,q}(1) + \\ \qquad \alpha_{p,q}(1,2) \cdot Moj_{p,q}(2) + \cdots + \\ \qquad \alpha_{p,q}(1,N_\rho) \cdot Moj_{p,q}(N_\rho) \\ \\ RFT_\theta(2) = \alpha_{p,q}(2,1) \cdot Moj_{p,q}(1) + \\ \qquad \alpha_{p,q}(2,2) \cdot Moj_{p,q}(2) + \cdots + \\ \qquad \alpha_{p,q}(2,N_\rho) \cdot Moj_{p,q}(N_\rho) \\ \\ \cdots \qquad\qquad \cdots \\ \\ RFT_\theta(N_\rho) = \alpha_{p,q}(N_\rho,1) \cdot Moj_{p,q}(1) + \\ \qquad \alpha_{p,q}(N_\rho,2) \cdot Moj_{p,q}(2) + \cdots + \\ \qquad \alpha_{p,q}(N_\rho,N_\rho) \cdot Moj_{p,q}(N_\rho) \end{cases}$$

where :

- $RFT_\theta(\rho_i)$ is the value of sample ρ_i on projection $\theta = arctan\frac{q}{p}$ acquired with the RFT,

- $\alpha_{p,q}(i,j)$ defines B-Spline coefficient between two bins b_i and b_j,

- $Moj_{p,q}(b_i)$ is the Mojette bin b_i value.

The resolution of the system above recovers the $\#_{bins}(p,q)$ values of Mojette bins of the projection (p,q) from the N_ρ RFT values of the projection θ, where $\theta = arctan\frac{q}{p}$ and $\#_{bins}(p,q) = N_\rho$.

3.4 Triangularisation of the System

Previous idea consisted to get $N_\rho = \#_{bins}(p,q)$ RFT values to perform $\#_{bins}(p,q)$ Mojette bins. The linear system obtained can be unresolvable (some of them have an infinity of solutions). Because of the step of sampling, many projection lines on corners of the image are omitted with Mojette point of view because they don't cross a pixel on center. However, they can be measured in RFT domain. Figure 12 shows two bolded lines not considered by Mojette.
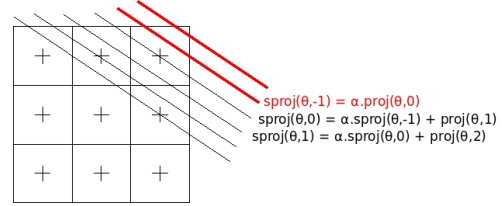

Figure 12: Omitted lines on a corner with Mojette's point of view

It is not necessary to process all omitted lines, but only those between the first Mojette line and the line which crosses only the first pixel. The number of lines to add before the first Mojette bin on a projection is defined by :

$$\#Lines(p,q) = \lceil \frac{(||p|-|q||) \cdot \sqrt{(p^2+q^2)}}{2p} \rceil \quad (7)$$
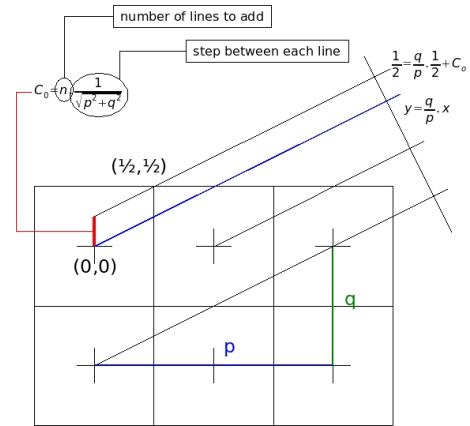
Figure 13: Determination of number of lines to add

Proof : Line equation on a projection (p,q) is $y = \frac{q}{p}x + c$. For the first pixel, $c = 0$. For the first line which only crossing the first pixel, we assume that $c = \frac{n}{\sqrt{p^2+q^2}}$, where n is the seeked number of lines and $\frac{1}{\sqrt{p^2+q^2}}$ is the step between each of them. This first line crosses at best the first pixel in position $(\frac{1}{2},\frac{1}{2})$ (Figure 13). We obtain equation 8. The ceiling of n gives the number of lines $\#Lines(p,q)$ to add.

$$\frac{1}{2} = \frac{q}{p} \cdot \frac{1}{2} + \frac{n}{\sqrt{p^2 + q^2}} \qquad (8)$$

The first line value depends on first Mojette bin value. The second one includes first and second Mojette bin values, and so on (Figure 12). The measure of these omitted lines allows to simplify the system above by a triangular system :

$$
\begin{cases}
Moj_{p,q}(0) = \frac{RFT_\theta(-n)}{\alpha_{p,q}(-n,0)} \\[2ex]
Moj_{p,q}(1) = \frac{RFT_\theta(-n+1) - Moj_{p,q}(0) \cdot \alpha_{p,q}(-n+1,0)}{\alpha_{p,q}(-n+1,1)} \\[2ex]
\dots \qquad \dots \\[2ex]
Moj_{p,q}(j) = \frac{RFT_\theta(j-n) - \sum_{k=j-2n \ge 0}^{k<j} Moj_{p,q}(k) \cdot \alpha_{p,q}(j,k)}{\alpha_{p,q}(j-n,j)} \\[2ex]
\dots \qquad \dots
\end{cases}
$$

where n is the number of added lines. Note that the denominator is the kernel representation between j and $j - n$. It can be fixed for a projection (p,q) by $c = \alpha_{p,q}(n,0)$.

The resolution of this triangular system links Radon and Mojette projections and recovers the Mojette bin values on each projection. Consequently, it allows a Mojette backprojection.

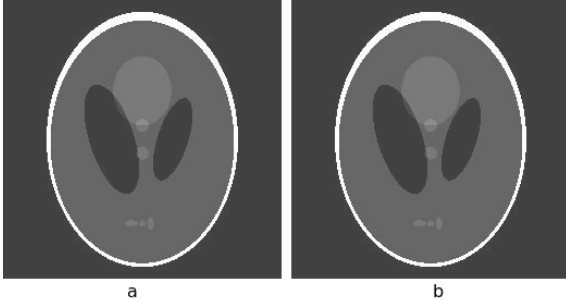# 4 RESULTS AND DISCUSSION

4.1 It is an exact reconstruction

Figure 14: (a) Original image, (b) Result of backprojection after triangular system resolution from RFT sinogram

Figure 14 shows the original image and the result of Mojette reconstruction from a RFT sinogram and linked by triangular systems of equations. Because of the fact that each angle of projection and step of values on a projection are determined by a couple (p,q), the RFT is equivalent to the Mojette transform (geometrically speaking). Furthermore, the linear system performs exactly Mojette bin values and finally, the reconstruction is exact.

The following table gives some error values between the original image exploited in this paper and results of reconstruction from different transforms.

	ΔC	ΔI	CC	MSE
RT^{-1}	-0.042	135.16	0.189	20473.
BFP	-0.015	70.50	0.345	6701.
RFT	0.00	0.00	1.00	0.00

Table 1: Comparisons of different methods

where :

- RT^{-1} is the usual Radon reconstruction,

- BFP is the Radon backprojection of filtered projections,

- RFT is the Mojette backprojection after triangular systems resolution from a B-Spline Radon sinogram piloted by a Farey series.

ΔC represents the difference of contrast C ($0 \le C \le 1$) between result and original images. ΔI is the difference of mean intensity ($0 \le I \le 255$). The coefficient of correlation $0 \le CC(I,J) \le 1$ shows the link between original and result images. Finally, usual mean squared error (MSE) values are given. Those results expose again exactness of Mojette backprojection from a RFT sinogram.

4.2 Interpolation and Results

However, the method above can't be adapted in practice in a X-Rays scan even if its geometry is compatible with physical acquisition. Indeed, even if it is easily acceptable to act on the angle step d_θ between each projection, it is more difficult to change the number and the step of projection lines for each one (it depends on sensors' disposition).

Consequently, we try now to perform an acquisition fully compatible with a scanner's one. The step of values (and consequently, the number of bins) is fixed for an entire acquisition according to the maximum number of bins necessary for a reconstruction (with Mojette) :

$$N_\rho = max\{\#_{bins}(p_i, q_i), (p_i, q_i) \in P\} \qquad (9)$$

$$d_\rho = \frac{1}{\sqrt{p_j^2 + q_j^2}} \text{ with } \#_{bins}(p_j, q_j) = N_\rho \qquad (10)$$

The projections of obtained $RRFT$ (Regular Radon Farey Transform) are more sampled than necessary for a Mojette backprojection using triangular systems. The RFT sinogram is derived from the $RRFT$ sinogram by linear interpolation between $RRFT$ values according to the geometrical properties of RFT. Triangular system resolutions and Mojette backprojection are obtained from this interpolated RFT sinogram. This reconstruction gives the result in figure 15.
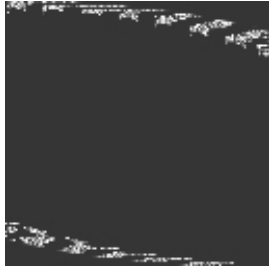
Figure 15: Result of backprojection from interpolated *RFT* sinogram

The Mojette transform is very sensitive to the noise in projections. The linear interpolation implies approximations in bins values. A small error on a bin value can be reverberated on the other bins during a backprojection step. Those others bins can also be noisy by the interpolation. Consequently, small errors can be propagated recursively and from bins to others and increase errors during the backprojection to give the result in figure 15.

However, the Mojette transform is also a mean for multiple description [9] of data because of the redundancy of informations between each projections. This characteristic allows to adapt error correcting methods to minimize errors on each projection. Our future works will consist to study which error correcting methods can be adapted for our reconstruction from an interpolated sinogram.

5 CONCLUSION AND PERSPECTIVES

The Radon transform is the essential method used in tomography to construct an image from a set of projections. The B-Spline kernel is more representative of a real scanner acquisition than the Dirac impulse because it allows to get continuous lines of projection where information is considered proportionnaly to the distance travelled through each pixel. However, irregular sampling gives approximations during the reconstruction.

On the other hand, the Mojette transform is an exact method in discrete domain but not adapted to an acquisition. However, guiding a B-Spline Radon acquisition with a Farey series to impose it with the same angles and the same number of bins allows to recover the Mojette projection by resolving a triangular equation system. Consequently, it is possible to reconstruct exactly an image with Mojette backprojection from a specifical B-Spline Radon acquisition.

However, this particular B-Spline Radon acquisition is not adjusted to a real acquisition because it implies a variable step of lines on each projection. We try to measure each projection with the same minimal line step necessary for Mojette backprojection and to interpolate

resulting sinogram to get it compatible with the triangular system and the Mojette backprojection. However, this interpolated sinogram is "noisy" by the interpolation and we are limited by the high noise sensitivity of the Mojette backprojection. Error correcting methods can be defined in Mojette domain to minimize errors in each bin by using the redundancy of informations contained in a Mojette sinogram. Our future works consist to study and to adapt those methods to obtain an efficient Mojette backprojection from a physical X-Rays acquisition.

REFERENCES

[1] Jean Pierre Guédon. *Les problèmes d'échantillonnages dans la reconstruction d'images à partir de projections*. PhD thesis, Université de Nantes, Ecole Nationale Supérieure de Mécanique, 1990.

[2] Jean Pierre Guédon and Yves Bizais. Bandlimited and Haar Filtered Back-Projection Reconstructions. *IEEE Transactions on Medical Imaging*, 13(3), September 1994.

[3] Jean Pierre Guédon and Nicolas Normand. Spline Mojette Transform : Applications in Tomography and Communications. *EUSIPCO*, 3:271–274, 2002.

[4] Jean-Pierre Guédon and Nicolas Normand. The Mojette Transform: The First Ten Years. pages 79–91, 2005.

[5] Gabor T. Herman and Attila Kuba. *Discrete Tomography - Foundations, Algorithms and Applications*. 1999.

[6] Stefan Horbelt, Michael Liebling, and Michael Unser. Discretization of the Radon Transform and of its Inverse by Spline Convolutions.

[7] Myron Bernard Katz. Questions of Uniqueness and Resolution in Reconstruction from Projections. *Lecture Notes in Biomathematics*, 1978. Springer-Verlag New York.

[8] Andrew Kingston and Imants Svalbe. Mapping Between Digital and Continuous Projections via the Discrete Radon Transform in Fourier Space. December 2003.

[9] B. Parrein, Nicolas Normand, and Jean-Pierre Guédon. Multiple Description Coding Using Exact Discrete Radon Transform. page 508, 2001.

[10] William H. Press. Discrete Radon Transform has an exact, fast inverse and generalizes to operations other than sums along lines. October 2006.

[11] Johann Radon. Uber die Bestimmung von Funktionen durch ihre Integralwerte langs gewisser Mannigfaltigkeiten. *Ber. Ver. Sachs. Akad. Wiss. Leipzig, Math-Phys. Kl*, 69:262–277, April 1917. In German. An ensligh translation can be found in

S. R. Deans : The Radon Transform and Some of Its Applications.

[12] Myriam Servieres. *Reconstruction tomographique Mojette*. PhD thesis, Université de Nantes, 2005.

[13] Claude Elwood Shannon. A Mathematical theory of communication. *The Bell System Technical Journal*, 27, July 1948.

[14] L. Shepp and B. Logan. The Fourier Reconstruction of a Head Section. *IEEE Transactions in Nuclear Science*, NS-21(2):21 – 43, 1974.

[15] Peter Toft. *The Radon Transform : Theory and Implementation*. PhD thesis, Department of Mathematical Modelling, Section for Digital Signal Processing, Technical University of Denmark, 1996.

[16] M. Unser, A. Aldroubi, and M. Eden. B-Spline signal processing: Part I—Theory. *IEEE Transactions on Signal Processing*, 41(2):821–833, February 1993. IEEE Signal Processing Society's 1995 best paper award.

[17] M. Unser, A. Aldroubi, and M. Eden. B-Spline signal processing: Part II—Efficient design and applications. *IEEE Transactions on Signal Processing*, 41(2):834–848, February 1993.

[18] Michael Unser, Akram Aldroubi, and Murray Eden. Polynomial Spline Signal Approximations : Filter Design and Asymptotic Equivalence with Shannon's Sampling Theorem. *IEEE Transactions on Information Theory*, 38(1), January 1992.